Received: 19 January 2024 | Accepted: 7 March 2024

DOI: 10.1097/HC9.0000000000000449

ORIGINAL ARTICLE

OPEN

BTLA deficiency promotes HSC activation and protects against hepatic ischemia-reperfusion injury

Xiaoyun Shen[1] | Rongyun Mai[2] | Xiao Han[2] | Qi Wang[1] | Yifan Wang[1] | Tong Ji[1] | Yifan Tong[1] | Ping Chen[1] | Jia Zhao[1] | Xiaoyan He[1] | Tong Wen[2] | Rong Liang[2] | Yan Lin[2] | Xiaoling Luo[2] | Xiujun Cai[1]

[1]Key Laboratory of Endoscopic Technology Research, Sir Run Run Shaw Hospital, Zhejiang University School of Medicine, Hangzhou, Zhejiang, P.R. China

[2]Department of Medical Oncology, Guangxi Medical University Cancer Hospital, Nanning, Guangxi, P.R. China

Correspondence
Xiujun Cai, Zhejiang University School of Medicine Sir Run Run Shaw Hospital, Zhejiang University School of Medicine, Hangzhou, Zhejiang, 310020, P.R. China.
Email: srrsh_cxj@zju.edu.cn

Xiaoling Luo, Guangxi Cancer Hospital and Guangxi Medical University, Affiliated Cancer Hospital, Nanning, Guangxi, 530021, P.R. China.
Email: luoxiaoling@gxmu.edu.cn

Abstract

Background and Aims: Hepatic ischemia-reperfusion injury (IRI) is unavoidable even despite the development of more effective surgical approaches. During hepatic IRI, activated HSC (aHSC) are involved in liver injury and recovery.

Approach and Result: A proportion of aHSC increased significantly both in the mouse liver tissues with IRI and in the primary mouse HSCs and LX-2 cells during hypoxia-reoxygenation. “Loss-of-function” experiments revealed that depleting aHSC with gliotoxin exacerbated liver damage in IRI mice. Subsequently, we found that the transcription of mRNA and the expression of B and T lymphocyte attenuator (BTLA) protein were lower in aHSC compared with quiescent HSCs. Interestingly, overexpression or knockdown of BTLA resulted in opposite changes in the activation of specific markers for HSCs such as collagen type I alpha 1, α-smooth muscle actin, and Vimentin. Moreover, the upregulation of these markers was also observed in the liver tissues of global BLTA-deficient ($BTLA^{-/-}$) mice and was higher after hepatic IRI. Compared with wild-type mice, aHSC were higher, and liver injury was lower in $BTLA^{-/-}$ mice following IRI. However, the depletion of aHSC reversed these effects. In addition, the depletion of aHSC significantly exacerbated liver damage in $BTLA^{-/-}$ mice with hepatic IRI. Furthermore, the TGF-β1 signaling pathway was identified as a potential mechanism for BTLA to negatively regulate the activation of HSCs in vivo and in vitro.

Abbreviations: aHSC, activated HSCs; ALT, alanine aminotransferase; AST, aspartate aminotransferase; BTLA, B and T lymphocyte attenuator; BTLA−/−, BLTA-deficient; CCL, chemokine ligand; COL1A1, collagen type I alpha 1; CTLA4, cytotoxic T lymphocyte Ag-4; CXCL1, C-X-C motif ligand 1; G-CSF, granulocyte colony–stimulating factor; HR, hypoxia-reoxygenation; HVEM, herpes virus entry mediator; IHC, immunohistochemistry; IR, ischemia-reperfusion; IRI, ischemia-reperfusion injury; mHSCs, mouse HSCs; qHSCs, quiescent HSCs; RNA-seq, RNA-sequencing; RT-PCR, real-time reverse transcription polymerase chain reaction; siRNAs, small interfering RNAs; TGF-β, transforming growth factor beta;TNF-α, tumor necrosis factor alpha; TUNEL, terminal deoxynucleotidyl transferase–mediated dUTP nick-end labeling; Vim, vimentin; α-SMA (ACTA2), α-smooth muscle actin.

Xiaoyun Shen, Rongyun Mai both authors contribute equally to this work.

Supplemental Digital Content is available for this article. Direct URL citations are provided in the HTML and PDF versions of this article on the journal’s website, www.hepcommjournal.com.

Conclusions: These novel findings revealed a critical role of BTLA. Particularly, the receptor inhibits HSC-activated signaling in acute IRI, implying that it is a potential immunotherapeutic target for decreasing the IRI risk.

INTRODUCTION

Hepatic ischemia-reperfusion injury (IRI) is a pathophysiologic process characterized by reperfusion and hypoxia in ischemic tissue during liver trauma, hemorrhagic shock, hepatectomy, and liver transplantation,[1,2] leading to hepatic failure, hemorrhagic shock, and graft dysfunction.[3,4] The acute phase of IRI is caused by an imbalance in the innate immune responses involving several immune cells, including macrophages, natural killer cells, dendritic cells, $CD4^+$ T cells, and $CD8^+$ T cells, causing a complex inflammation. Despite significant advancements in perioperative management and surgical techniques, the occurrence of hepatic IRI is difficult to prevent during liver surgery, which calls for further investigation into the mechanisms of liver IRI and develop new treatment methods.

HSCs are located in the perisinusoidal space between sinusoidal endothelial cells and hepatocytes and account for 5%–8% of the cells in the liver. Under health conditions, HSCs maintain a nonproliferation and quiescent phenotype.[5,6] However, upon liver injury, the quiescent HSCs (qHSCs) are quickly activated, transforming to be myofibroblast-like cells, also known as activated HSCs (aHSC), to participate in liver repair and regeneration after hepatectomy or into liver fibrosis during chronic liver injury.[7,8] Regarding hepatic IRI, the function of aHSC in liver injury and recovery is controversial. Hepatic IRI–activated aHSC seem to exacerbate acute liver injury by increasing the production of pro-inflammatory factors[9] and contribute to prolonged recovery time and extensive fibrosis.[10] However, Jameel et al[11] found that aHSC release powerful antioxidant proteins that protect the liver from hepatic IRI. Konishi et al[12,13] proposed that hepatic recovery and regeneration after liver IRI depend on the HSC proliferation and activation, and the liver fibrosis induced by this process cannot enhance the susceptibility of hepatic to subsequent liver damage. Therefore, understanding the role of aHSC in liver IRI could eliminate the controversy surrounding the role of aHSC in liver IRI and provide methods for promoting liver recovery.

B and T lymphocyte attenuator (BTLA), a co-inhibitory receptor like programmed death 1 (PD1) and cytotoxic T lymphocyte ag-4 (CTLA4), is a member of the CD28 immunoglobulin superfamily and is mainly involved in the negative regulation of various immune cell activation and proliferation.[14,15] The BTLA ligand is the herpes virus entry mediator (HVEM), a member of the TNF receptor superfamily rather than the classical B7 family.[16,17] The BTLA/HVEM signaling axis is involved in many physiological and pathological processes, such as the pathogenesis of tumors, inflammatory diseases, autoimmune diseases, infectious diseases, and transplant rejection.[17] A combination of BTLA and HVEM directly links the CD28 and TNF receptor families, inhibiting the overactivation of lymphocytes in vivo and preventing autoimmune injury. However, in tumor tissues, the abnormal expression of HVEM can inhibit the immune function of cytotoxic killer lymphocytes by binding with BTLA, resulting in immune evasion and tumor progression.[18,19] Studies have shown that activation of co-inhibitory receptors can effectively regulate organ damage caused by inflammation. Ji et al[20] proposed that the upregulation of PD1 signals can greatly alleviate liver IRI–induced inflammation and injury by promoting the inactivation of T cells and disputing the function of KDs. Takada et al[21] and Chandraker et al[22] suggested that CTLA4 Ig could protect the kidney from renal IRI. Although no direct evidence of the functions of BTLA in liver IRI exists, our study showed the involvement of BTLA in liver IRI. To illustrate this, we constructed a mouse hepatic IRI model on wild-type and BLTA-deficient ($BTLA^{-/-}$) mice and compared the degree of liver damage and HSC activation. We found that downregulation of BTLA alleviated the severity of liver injury in the hepatic IRI model by activating HSCs, providing a potential option for treating liver IRI and preventing subsequent adverse reactions.

EXPERIMENTAL PROCEDURES

Mice

C57BL/6 mice aged 8–10 weeks and weighing ~25 ± 2 g were purchased from the Laboratory Animal Center of Zhejiang University School of Medicine (Hangzhou, China). The mice were housed in a temperature-controlled, pathogen-free facility with a 12-hour (h) light/dark cycle and free access to food and water. All procedures were performed with the protocols approved by the Experimental Animal Welfare Ethics Review Committee of Zhejiang University (Project Approval Number: ZJU20170115) and were conducted following the guidelines outlined by the Guide for the Care and Use of Laboratory Animals published by the National Institutes of Health (Publication 86-23, revised 1985). $BTLA^{-/-}$ mice were purchased from Biocytogen Pharmaceuticals (Beijing) Co., Ltd., and generated by the CRISPR/Cas9 system (Supplemental Figure 1a, http://links.lww.

com/HC9/A909). Primer sequences of BTLA are listed in Supplemental Table 1, http://links.lww.com/HC9/A910.

Mouse warm hepatic IRI model

The nonfatal segmenting (~70%) liver warm IRI model was performed as represented.[23] In brief, mice were anesthetized with pentobarbital sodium (50 mg/kg) i.p. injection, and each layer was dissected vertically to expose the liver. All structures in the left and median liver lobes of portal triple ducts were blocked for 90 minutes with a microvascular clamp (Supplemental Figure 1b, http://links.lww.com/HC9/A909); reperfusion begins by removing the clamp. The mice were sacrificed 6 hours or 24 hours after reperfusion, and the serum and liver tissues were harvested for further analyses. In addition, the same operation procedure was performed in the sham-operated group, but not blocked.

Mouse aHSC depletion

In this study, we used gliotoxin to deplete aHSC in mice, as described.[24,25] In brief, mice were injected intraperitoneally with either gliotoxin (3 mg/kg; Yuanye Bio-Technology, Shanghai) or (DMSO; vehicle control) 24 hours before IR and immediately after operation.

Primary mouse HSC isolation

Male C57BL/6 mice between 24 and 26 weeks of age were anesthetized with deep anesthesia. Retrograde perfusion through the inferior vena cava was followed by EGTA (Sigma) solution for 2 minutes, D-hanks solution (Solarbio) for 2 minutes, and collagenase IV (Sigma) solution for 15 minutes, outflow from the portal vein, always clamping the superior hepatic vena cava (Supplemental Figure 1c, http://links.lww.com/HC9/A909). After rapid separation of the liver, primary mouse HSCs were isolated by collagenase perfusion and followed by density gradient centrifugation, as reported.[26] Finally, HSCs were isolated and cultured in a humidified incubator (95% air, 5% CO_2) at 37°C, with a high-glucose DMEM (Invitrogen) containing 10% fetal bovine serum (Gibco) and 1% penicillin/streptomycin (*P*/S; meilunbio). After about 12 hours of incubation, fresh complete DMEM was replaced to remove necrotic floating cells, which remained as qHSCs, and the culture was continued until day 5 to establish aHSC.

Cell line culture

The human HSC line (LX-2) was purchased from the China Center for Type Culture Collection (GPC0076, CCTCC, China). All cells were cultured in DMEM containing 100 ng/mL streptomycin (CellMax, USA), 100 U/mL penicillin (CellMax, USA), and 10% fetal bovine serum (CellMax, USA) in a 5% CO2 humidified incubator at 37°C.

RNA interference and overexpression

LX-2 cells were transfected by Lipofectamine™ 3000 Transfection Reagent (Invitrogen, USA) based on the manufacturer's instructions. For RNA interference, the LX-2 cells were transfected with negative control short interfering RNAs (siNC) or BTLA siRNA (#1: GAACCATTCTGTCATTGGA; #2: CCAACAGAATATGCATCCA; Ribobio, China). For overexpression, the LX-2 cells were transfected with 2 μg of pcDNA3.1-empty vector or pcDNA3.1-BTLA (Shanghai Hanyin Biotech Co.). Opti-MEM was transfected with Lipofectamine™ 3000 reagent for 12 hours, and the medium was then replaced into complete DMEM for 48 hours or 72 hours to prepare for subsequent experiments.

Hypoxia-reoxygenation (HR) model

HR model was used to mimic hepatic IRI in vitro, as reported.[27] Briefly, the cells were first cultured in a hypoxia incubator chamber (1% O_2, 5% CO_2, and 94% N_2) with glucose-free and serum-free DMEM for 6 hours, and replaced to complete DMEM and cultured in the normal culture condition (95% air, 5% CO_2) for another 6 hours to prepare for subsequent experiments.

Liver function assessment

Mouse blood samples were placed at 37°C for 1 hour, and then serum was collected after centrifuged at 3000 rpm for 10 minutes. The activities of serum levels of alanine aminotransferase (ALT) and aspartate aminotransferase (AST) were determined using AST/ALT/GPT Assay Kit (Nanjing Jiancheng Biological Technology, China) following the manufacturer's instructions.

Measurement of inflammatory cytokines and chemokines

The method of collecting mice serums was described above. The levels of inflammatory cytokines in the serum of mice were measured by a commercial LEGENDplex™ Multi-Analyte Flow Assay Kit (Biolegend® Enabling Legendary Discovery™) for flow cytometry in accordance with the manufacturer's protocols.

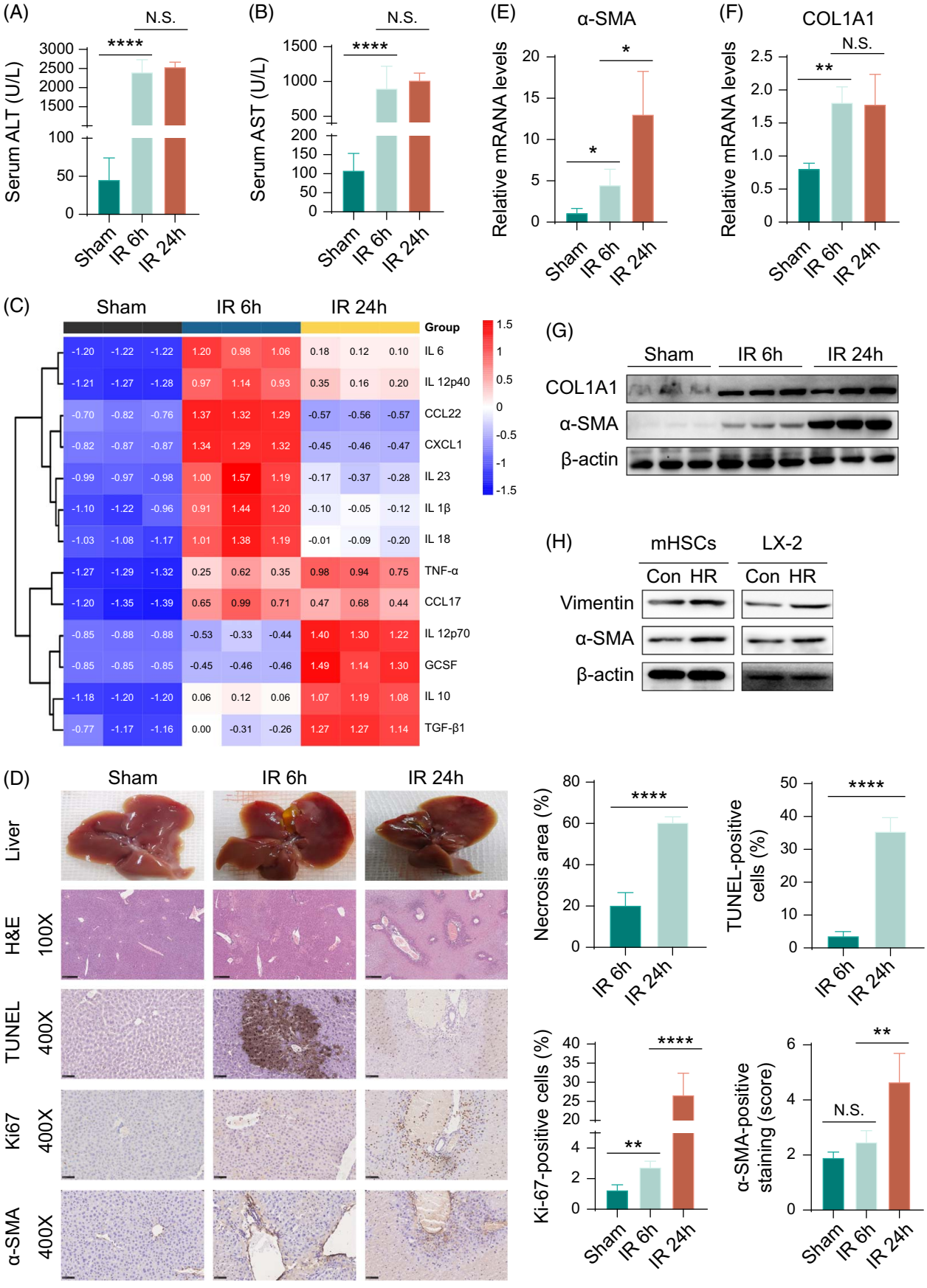
(A)
Serum ALT (U/L)
N.S.
****
Sham
IR 6h
IR 24h
(B)
Serum AST (U/L)
N.S.
****
(E)
α-SMA
Relative mRANA levels
*
(F)
COL1A1
N.S.
**
(C)
Sham
IR 6h
IR 24h
Group
IL 6
IL 12p40
CCL22
CXCL1
IL 23
IL 1β
IL 18
TNF-α
CCL17
IL 12p70
GCSF
IL 10
TGF-β1
(G)
COL1A1
α-SMA
β-actin
(H)
mHSCs
LX-2
Con HR
Vimentin
(D)
Liver
H&E
100X
TUNEL
400X
Ki67
α-SMA
Necrosis area (%)
TUNEL-positive cells (%)
Ki-67-positive cells (%)
α-SMA-positive staining (score)

FIGURE 1 The effect of IRI on HSC activation. The level of (A) ALT, (B) AST, and (C) inflammatory cytokines in livers of those subjected to IRI and control group. (D) The morphology (necrotic change), H&E staining (magnification × 100), TUNEL staining (brown color indicative of necrosis/apoptosis; magnification × 400), Ki-67 staining (brown color indicative of proliferation; magnification × 400), and α-SMA staining (brown color indicating aHSC deposition; magnification × 400) analyses of livers from wild-type mice IRI (n = 4–5/group). (E) and (F) qPCR analysis for the mRNA of α-SMA and COL1A1. (G) Western blot analysis for the expression of COL1A1 and α-SMA in livers of wild-type mice subjected to IRI (n = 3/group); (H)Western blot analysis for the expression of Vimentin and α-SMA in primary mouse HSCs (mHSCs) and LX-2 cells after HR stimulation; All data are presented as the mean ± SD, * $p < 0.05$, ** $p < 0.01$, *** $p < 0.001$, **** $p < 0.0001$. Abbreviations: aHSC, activated HSCs; ALT, alanine aminotransferase; AST, aspartate aminotransferase; COL1A1, collagen type I alpha 1; Con, control; H&E, hematoxylin and eosin; HR, hypoxia-reoxygenation; IRI, ischemia-reperfusion injury; mHSCs, mouse HSCs; N.S., nonsignificant; RT-PCR, real-time reverse transcription polymerase chain reaction; α-SMA (ACTA2), α-smooth muscle actin; Vim, Vimentin.

RT-qPCR

The fresh liver samples were homogenized through a QIAshredder spin column (Jingxin, China). Total RNA was isolated from hepatic samples or cells using the RNA-Quick Purification Kit (Shanghai Yishan Biotechnology Co., Ltd.) according to the manufacturer's instructions. Complementary DNA was synthesized using Hifair® II 1st Strand cDNA Synthesis SuperMix (Shanghai Yishan Biotechnology Co., Ltd.) for qPCR, and then the RT-qPCR assay was detected by FastStart Universal SYBR Green Master Rox (Roche Ltd.) to quantify mRNA levels. The primers for RT-qPCR were synthesized by TsingKe Biological Technology. The relative gene expression data were calculated by the $2^{-\Delta\Delta Ct}$ algorithm,[28] and all determinations were repeated 3 times. Primer sequences of related genes are listed in Supplemental Table 1, http://links.lww.com/HC9/A910.

Histopathological analysis

Gross morphology and hematoxylin and eosin staining were applied to estimate the liver necrosis degree. Mice hepatic samples were fixed in 4% phosphate-buffered formalin at 37°C shakings overnight, and then dehydrated, embedded in paraffin, and sliced to 4 μm–5 μm slides. According to the manufacturer's instructions, the slides were then dewaxed and stained with Hematoxylin and Eosin Staining Kit (Solarbio, China). As for immunohistochemistry (IHC) staining, the slides were first dewaxed and the Ag was retrieved, then 10% bovine serum albumin was used at 37°C for 1 hour to block the nonspecific antibody. After incubating with the primary antibody at 4°C overnight, the secondary antibody conjugated with horseradish peroxidase was appropriately added and incubated at 37°C for 30 minutes. After washing with phosphate buffer saline, according to the manufacturer's protocols, slides were processed by the GTvision immunohistochemistry kit (Shanghai GeneTech Company Limited). Lastly, color reaction was performed to show the chemical constituents of tissues or cells observed under the light microscope, and the staining density (0–3 points: negative staining, light yellow, pale yellow, dark brown) and the positive rate (1–4 points: 0%–25%, 26%–50%, 51%–75%, 76%–100%) were scored. The product of staining intensity and staining density is the final score of the sample. All antibodies used in this study are listed in Supplemental Table 2, http://links.lww.com/HC9/A910.

TUNEL staining

Hepatocyte apoptosis in paraffin-embedded slides was measured by the TUNEL kit (Nanjing KeyGen Biotech Co., Ltd.) following the manufacturer's instructions. The TUNEL-positive cells were observed by light microscope and counted the number in 5 randomly selected × 200 fields on each slide.

Western blot analysis

Total protein was extracted by adding protease inhibitors (MedChemExpress) and phosphatase inhibitors (MedChemExpress) with RIPA lysis buffer (Beyotime Institute of Biotechnology). Hepatic tissues or cells were lysed in protein lysis buffer on ice and the protein concentrations were detected by a bicinchoninic acid protein assay kit (Meilunbio, China). The proteins were separated with sodium dodecyl sulfate-polyacrylamide gel electrophoresis and then transferred onto a polyvinylidene fluoride membrane (Millipore, USA). After blocking the membrane with skim milk on the rocking shaker for 1 hour, appropriate concentration of primary antibody was added, and then incubated in the shaker at 4°C overnight. The membrane was then rinsed drastically in washing buffer the next day and incubated with horseradish peroxidase-conjugated secondary antibody for 1 hour. Finally, enhanced chemiluminescence reagents (Fdbio Science, China) were applied to evaluate the Ag-antibody complex on the membrane. The bands were detected using the ChemiDoc™ Touch Imager (Bio-Rad Laboratories, Inc.) and analyzed by ImageLab software version 5.2 (Bio-Rad Laboratories, Inc.). All antibodies used in this research are listed in Supplemental Table 2, http://links.lww.com/HC9/A910.

RNA-seq and data analysis

Primary mouse qHSCs and aHSC were obtained according to the method mentioned above, and RNA was

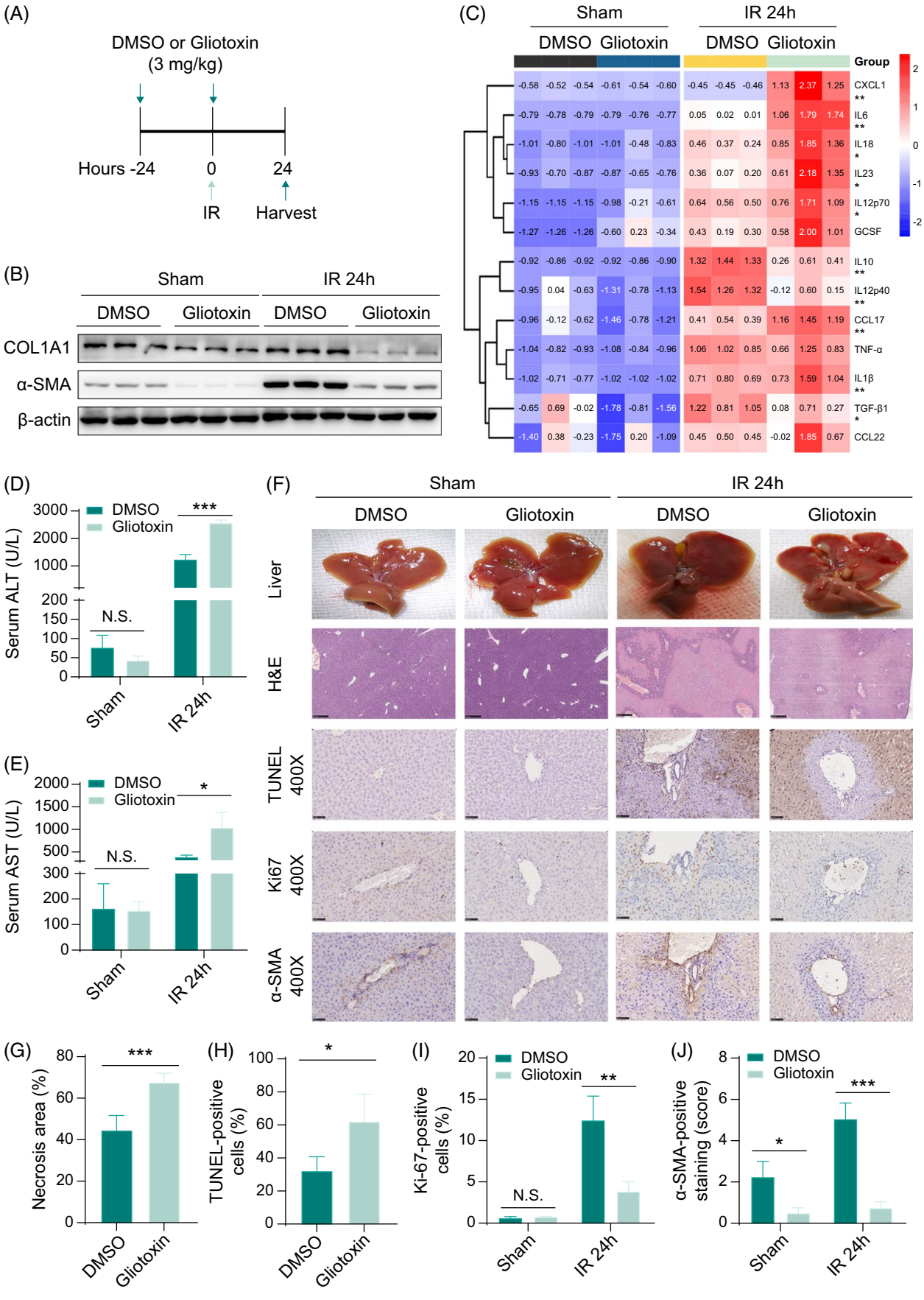
(A)
DMSO or Gliotoxin
(3 mg/kg)
Hours -24
0
24
IR
Harvest
(B)
Sham
IR 24h
DMSO
Gliotoxin
DMSO
Gliotoxin
COL1A1
α-SMA
β-actin
(C)
Sham
IR 24h
DMSO Gliotoxin
DMSO Gliotoxin
Group
CXCL1 **
IL6 **
IL18 *
IL23 *
IL12p70 *
GCSF
IL10 **
IL12p40 **
CCL17 **
TNF-α
IL1β **
TGF-β1 *
CCL22
(D)
Serum ALT (U/L)
DMSO
Gliotoxin
***
N.S.
Sham
IR 24h
(E)
Serum AST (U/L)
DMSO
Gliotoxin
*
N.S.
Sham
IR 24h
(F)
Sham
IR 24h
DMSO
Gliotoxin
DMSO
Gliotoxin
Liver
H&E
TUNEL 400X
Ki67 400X
α-SMA 400X
(G)
Necrosis area (%)
***
DMSO
Gliotoxin
(H)
TUNEL-positive cells (%)
*
DMSO
Gliotoxin
(I)
Ki-67-positive cells (%)
DMSO
Gliotoxin
**
N.S.
Sham
IR 24h
(J)
α-SMA-positive staining (score)
DMSO
Gliotoxin
*
***
Sham
IR 24h

FIGURE 2 Effects of aHSC on the apoptosis and proliferation of hepatocytes during IRI. (A) Schematic diagram of depletion of aHSC in mice, in which wild-type mice were treated with DMSO or 3 mg/kg gliotoxin, followed by a second dose 24 hours later at the time of hepatic IR. Livers were harvested 24 hours following treatment. (B)Western blot analysis for the expression of COL1A1 and α-SMA in livers of wild-type mice (n = 3/group). (C) Flow cytometry analysis for the levels of serum inflammatory cytokines and chemokines in livers of wild-type mice. (D) and (E) ALT and AST in serum from wild-type mice (n = 3–4/group). (F) Gross morphology (necrotic change), H&E staining (magnification × 100), TUNEL staining (brown color indicative of necrosis/apoptosis; magnification × 400), Ki-67 staining (brown color indicative of proliferation; magnification × 400), and α-SMA staining (brown color indicating aHSC deposition; magnification × 400) analyses for livers from wild-type mice. (G), (H), (I), and (J) Corresponding quantitative analyses of immunohistochemistry. All data are presented as the mean ± SD, * $p < 0.05$, ** $p < 0.01$, *** $p < 0.001$, **** $p < 0.0001$. Abbreviations: aHSC, activated HSCs; ALT, alanine aminotransferase; AST, aspartate aminotransferase; COL1A1, collagen type I alpha 1; H&E, hematoxylin and eosin; IR, ischemia-reperfusion; N.S., nonsignificant; α-SMA (ACTA2), α-smooth muscle actin.

extracted from these cells for subsequent RNA-sequencing (RNA-seq) and analysis by Hangzhou Lianchuan Biotechnology Co., Ltd. Briefly, following purification, a final cDNA library was established by the mRNA-Seq sample preparation kit (Illumina, San Diego, USA) based on the manufacturer's instructions. The transcriptome was sequenced by the Illumina paired-end RNA-seq method. Reads from primary mouse qHSCs and aHSC were then compared with the University of California Santa Cruz (http://genome.ucsc.edu/) Mus musculus reference genome by the HISAT software package, and assembled through StringTie. Next, Perl script was hired to merge all the transcripts to rebuild a comprehensive transcriptome. Finally, the levels of all transcripts in the final transcriptome were assessed using StringTie and Ballgown. The differentially expressed mRNAs were screened out with statistical significance ($|\text{fold change}| > 1.5$ and $p < 0.05$). Advanced heat map and volcano plot were plotted by the OmicStudio tools (https://www.omicstudio.cn/tool).

Statistical analysis

All data are presented as means ± SE. Two-tailed Student's *t*-test (2 groups) and one-way ANOVA (multiple groups) were used for comparisons. $p < 0.05$ was considered to be statistically significant. Analysis and graphing were carried out through the GraphPad Prism software (version 9.0).

RESULTS

HSC activation increased significantly in both in vivo and in vitro hepatic IRI

To explore the relationship between aHSC and liver IRI, we created a mouse model of warm 70% liver IRI with ischemia for 90 minutes and reperfusion for 6 hours or 24 hours. Serum ALT and AST levels revealed impaired liver function (Figure 1A, B), while hematoxylin and eosin staining revealed severe hepatic tissue necrosis (Figure 1D). Since inflammation, apoptosis, and proliferation of hepatocytes are involved in liver injury and recovery during hepatic IRI,[29] we compared the levels of inflammatory cytokines (TNF-α, IL-1β, IL-6, IL-10, IL-12 p70, IL-12p40, IL-18, IL-23, G-CSF, and TGF-β1) and chemokines (chemokine ligand [CCL]17, CCL22, and C-X-C motif ligand 1 [CXCL1]), the apoptosis, and the proliferation of hepatocytes between the IRI and non-IRI groups separately. The expression of inflammatory cytokines and chemokines, apoptosis, and proliferation of cells was found to be higher in these experimental mice (Figure 1C, D). These results confirmed the successful establishment of the hepatic IRI mouse model. In addition, during the injury phase, the liver injury gradually worsened and was significantly aggravated 24 hours after reperfusion. Liver injury is accompanied by the recovery of the liver, and this antagonistic repair response appeared at the early stage of injury and gradually intensified.

Coincidentally, we observed an increase in the transcription of mRNA (Figure 1E, F) and protein expression (Figure 1G, Supplemental Figures 2e, 2f, http://links.lww.com/HC9/A911) of alpha-smooth muscle actin (α-SMA) and collagen type I (COL1A1), both markers for aHSC, in the liver after IRI. These results suggest that IRI stress induced the transformation of qHSCs into aHSC. Furthermore, IHC staining showed that hepatic parenchyma and periportal zones around the necrotic area have more α-SMA-positive HSCs, accompanied by fewer apoptotic hepatocytes but many proliferating cells in the liver at 24 hours after reperfusion (Figure 1D). These findings suggest that αHSC may regulate hepatocyte injury and regeneration after IRI. Finally, whether hepatic IRI induces the activation of HSCs through primary mouse HSC (mHSCs) and LX-2 cells was investigated. After stimulating the HR cell model, the morphology of mHSCs changed from star-shaped to extended dendritic cell processes and formed clusters and fibers (Supplemental Figure 2g, http://links.lww.com/HC9/A911), and the levels of α-SMA and vimentin (Vim) (another aHSC marker) were significantly high in both mHSCs and LX-2 cells (Figure 1H, Supplemental Figures 2a-2d, http://links.lww.com/HC9/A911). These results further confirmed that hepatic IRI stress could activate HSCs.

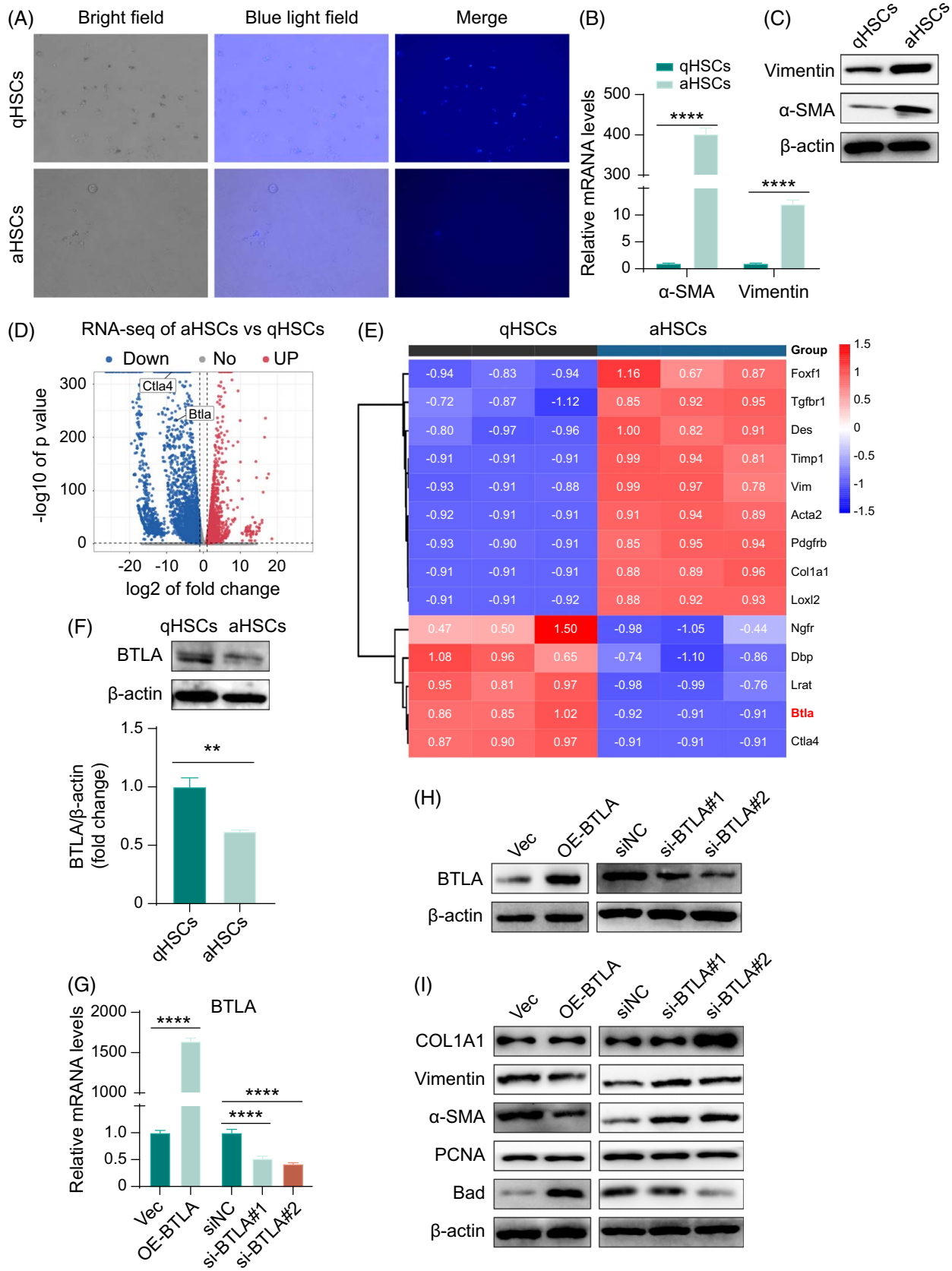

FIGURE 3 BTLA expression was significantly decreased after HSC activation in vitro. (A) Inverted fluorescence microscope shows that most qHSCs store vitamin A–containing lipid droplets, which give the qHSCs a feature of fading blue autofluorescence, while aHSC lose lipid droplets (magnification ×200). (B) RT-qPCR and (C) western blot analysis of Vimentin and α-SMA mRNA and protein expression in qHSCs

and aHSC. (D) Volcanic map showing the RNA-seq analysis results of primary mouse qHSCs and aHSC, including 3256 upregulated genes and 3380 downregulated genes, among which BTLA and CTLA4, 2 members of CD28 family, were significantly downregulated after primary mouse HSC activation. (E) Heat map analysis of selected genes, with well-known genes associated with aHSC and qHSCs markers, as well as BTLA and CTLA4. (F) Western blot analysis and quantification results of BTLA expression in primary mouse qHSCs and aHSC. (G) RT-qPCR analysis, and (H) Western blot analysis of transfection efficiency of BTLA in LX-2 cells (human aHSC cell line) following transfection with empty-vector control or siNC, and transfected with BTLA overexpression or siRNAs (siBTLA#1 and siBTLA#2); (I) Western blot showing expression of aHSC markers (COL1A1, Vimentin, α-SMA), proapoptotic gene (Bad) and proliferation gene (PCNA) in LX-2 cells transfected with empty-vector control or siNC, and transfected with BTLA overexpression or siRNAs (siBTLA#1 and siBTLA#2). All data are presented as the mean ± SD, * $p < 0.05$, ** $p < 0.01$, *** $p < 0.001$, **** $p < 0.0001$. Abbreviations: aHSC, activated HSCs; BTLA, B and T lymphocyte attenuators; COL1A1, collagen type I alpha 1; CTLA4, cytotoxic T lymphocyte ag-4; N.S., nonsignificant; PCNA, proliferating cell nuclear antigen; qHSCs, quiescent HSCs; RT-PCR, real-time reverse transcription polymerase chain reaction; RNA-seq, RNA-sequencing; α-SMA (ACTA2), α-smooth muscle actin; Vim, Vimentin.

HSC activation protects the liver from hepatic IRI

Next, whether the HSC activation after hepatic IRI is detrimental or beneficial to liver recovery and repair was assessed by depleting aHSC with gliotoxin (an anti-fibrotic fungal metabolite known to induce aHSC apoptosis[24,25]). The mice were injected i.p. with either 3 mg/kg gliotoxin or DMSO 24 hours before hepatic IR and immediately after operation (Figure 2A). Gliotoxin treatment significantly downregulated the levels of α-SMA and COL1A1 under both normal physiological conditions and hepatic IRI stress (Figure 2B, Supplemental Figures 2h, 2i, http://links.lww.com/HC9/A911). IHC staining of α-SMA confirmed these results (Figure 2F, J), indicating the successful depletion of aHSC by gliotoxin in mice.

Further liver damage assessments were performed. No difference in liver function, inflammatory cytokines and chemokines, necrotic area, apoptotic cells, and proliferating cells were observed between the gliotoxin-treated group and the DMSO-treated sham group, indicating that the gliotoxin dose did not cause liver injury under normal physiological conditions (Figure 2C, F-I). However, severe liver damage, higher serum ALT/AST levels (Figure 2D, E), higher levels of pro-inflammatory cytokines (IL-6, IL-18, IL-23, IL-12P70, and IL-β), higher levels of chemokines (CXCL1 and CCL17), larger necrotic area and more hepatocytes apoptosis, but lower anti-inflammatory cytokines (IL-10 and TGF-β1) and lower proliferation of cells (Figure 2C, F-I) were observed in the hepatic IRI group treated with gliotoxin. Contrary to the phenomenon of α-SMA expression in HSCs induced by IRI, IHC staining revealed more apoptotic hepatocytes and fewer proliferating cells in the periportal zone region after depletion of aHSC by gliotoxin (Figure 2F). These results suggest that depletion of aHSC exacerbates liver injury during hepatic IR.

Taken together, these results revealed that activation of HSCs in the liver induced by IRI is a reparative protective response in regulating the recovery and regeneration after IRI.

BTLA decreased significantly after the activation of primary mHSCs

To investigate the molecular mechanisms involved in the activation of HSCs, we isolated and purified primary mHSCs and then cultured them in a complete DMEM for five days. As previously reported,[4] most qHSCs store vitamin A–containing lipid droplets, which gives qHSCs a fading blue-green autofluorescence appearance. However, aHSC will lose their lipid droplets (Figure 3A). Further, the mRNA transcription and expression of Vim and α-SMA protein were remarkably higher in aHSC (Figure 3B, C, Supplemental Figure 3a, http://links.lww.com/HC9/A912), demonstrating the successful establishment of primary mouse aHSC. RNA-seq analysis of primary mouse qHSCs and aHSC was then performed to identify potential genes involved in the activation of HSCs. Results showed that the expression of 3256 genes was upregulated, whereas that of 3380 genes was downregulated in aHSC compared with qHSCs ($|\text{fold change}| > 1.5$ and $p < 0.05$; Figure 3D). Among them, certain αHSC markers, such as TIMP1, α-SMA (ACTA2), COL1A1, Vim, PDGF receptor beta, lysyl oxidase-like 2, TGF beta receptor 1, forkhead box F1, and desmin, were significantly upregulated in aHSC. In contrast, certain markers for qHSCs, such as lecithin-retinol acyltransferase, nerve growth factor receptor, and D site albumin promoter–binding protein, were down-expressed in aHSC (Figure 3E). As described in the Introduction section, members of the CD28 family are involved in liver IRI. Thus, we compared the levels of CD28 in the 2 groups. The results showed that BTLA and CTLA4 were significantly lowest in aHSC (Figure 3E). RT-qPCR analysis revealed comparable findings. Furthermore, we observed that BTLA was one-fold lower than CTLA4 in primary mouse aHSC (Figure 3E, Supplemental Figure 3b, http://links.lww.com/HC9/A912). Western blot analysis further identified that BTLA protein was downregulated in the primary mouse aHSC (Figure 3F). In light of these findings, we hypothesized that downregulated BTLA may contribute to the activation of HSCs.

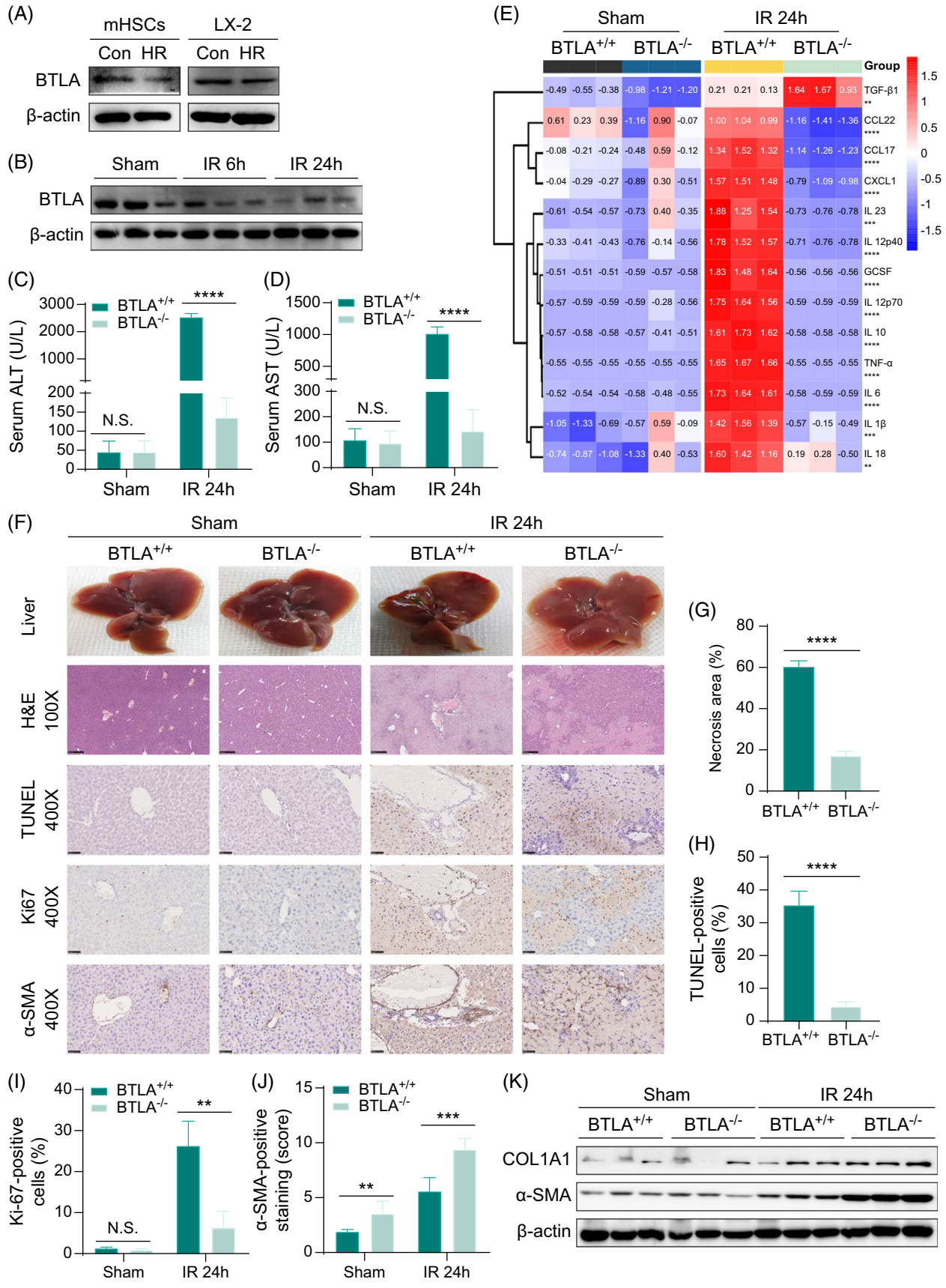

FIGURE 4 BTLA was significantly downregulated in liver IRI, whereas BTLA deficiency significantly reduced liver injury and promoted HSC activation during IRI. (A) Western blot analysis of BTLA expression in primary mouse HSCs (mHSCs) and LX-2 cells subjected to control or HR

stimulation. (B) Western blot showing BTLA expression in liver tissues from wild-type mice subjected to sham treatment or IRI (n = 3/group). Serum (C) ALT and (D) AST in livers from $BTLA^{+/+}$ mice or $BTLA^{-/-}$ mice subjected to sham treatment or IRI (n = 3–4/group). (E) Flow cytometry analysis of serum inflammatory cytokines and chemokines levels in liver tissues from wild-type mice or BTLA-deficient (BTLA−/−) mice. (F) The gross morphology (necrotic change), H&E staining (magnification × 100), TUNEL staining (brown color indicative of necrosis/apoptosis; magnification × 400), Ki-67 staining (brown color indicative of proliferation; magnification × 400), and α-SMA staining (brown color indicating aHSC deposition; magnification × 400) of liver tissues from wild-type mice or BTLA−/− mice; (G), (H), (I), and (J) The corresponding quantitative analysis results. (K) Western blot showing expression of COL1A1 and α-SMA in liver tissues from wild-type mice or BTLA−/− mice (n = 3/group). All data are presented as the mean ± SD, * $p < 0.05$, ** $p < 0.01$, *** $p < 0.001$, **** $p < 0.0001$. Abbreviations: aHSC, activated HSCs; ALT, alanine aminotransferase; AST, aspartate aminotransferase; BTLA, B and T lymphocyte attenuators; BTLA−/−, BLTA-deficient; COL1A1, collagen type I alpha 1; IR, ischemia-reperfusion; mHSCs, mouse HSCs; N.S., nonsignificant; α-SMA (ACTA2), α-smooth muscle actin.

BTLA is involved in negatively regulating HSC activation in vitro

To investigate the effect of BTLA on the biological properties of HSCs, we constructed BTLA overexpressing or knockdown cells using LX-2 cells (Figure 3G-H, Supplemental Figure 3d, http://links.lww.com/HC9/A912). As shown in Figure 3I and Supplemental Figures 3e-3i, http://links.lww.com/HC9/A912, the expression of Bad, a proapoptotic protein, increased dramatically in cells overexpressing BTLA. In contrast, the expression of proliferating cell nuclear antigen showed that BTLA had no effect on the proliferation of LX-2 cells. Moreover, the expression of specific markers for aHSC (COL1A1, Vim, and α-SMA) was detected to assess the activation status of LX-2 cells. Compared to empty vector control cells, the results showed that the activation of LX-2 cells with BTLA overexpression was significantly reduced. These findings were further confirmed by BTLA knockdown in LX-2 cells. These data suggest that BTLA is likely to be a negative regulator of HSC activation.

BTLA is significantly downregulated both in vivo and in vitro hepatic IRI

BTLA is vital in immunity and inflammatory response.[14,30] However, its function in liver IRI is still unclear. Therefore, we analyzed the expression of BTLA in IRI mice. It was found that the levels of BTLA in the hepatic tissues of mice decreased significantly after IRI (Figure 4B, Supplemental Figure 4c, http://links.lww.com/HC9/A913). We also found that HR model stimulation significantly reduced the expression of BTLA protein in mHSCs and LX-2 cells (Figure 4A, Supplemental Figures 4a, 4b, http://links.lww.com/HC9/A913). These results preliminarily indicated that hepatic IRI inhibited the expression of BTLA and promoted the activation of HSCs.

BTLA deficiency significantly alleviates liver injury and regulates the activation of HSCs during hepatic IRI in vivo

To further determine the effect of BTLA on hepatic IRI, we constructed and confirmed $BTLA^{-/-}$ mice confirmed by genotyping and western blot analyses (Supplemental Figure 1a, http://links.lww.com/HC9/A909, Supplemental Figures 4d-4f, http://links.lww.com/HC9/A913). We found no significant changes in liver function and hepatic structures between $BTLA^{-/-}$ mice and normal control mice. However, the serum ALT and AST levels dramatically decreased in the $BTLA^{-/-}$ mice after liver IRI (Figure 4C, D). The expression of inflammatory cytokines (TNF-α, IL-6, IL-1β, IL-10, IL-18, IL-23, IL-12p40, and IL-12p70) and chemokines (CXCL1, CCL17, and CCL22) showed a similar trend. However, the expression of anti-inflammatory cytokines (TGF-β1) was significantly increased (Figure 4E). The above events were accompanied by mild hepatic necrosis and hepatocyte apoptosis. The necrotic area decreased from ~60% to nearly 15%, and the apoptosis of liver cells decreased from about 35% to almost 5% after IRI (Figure 4F-H). In addition, Ki-67 IHC staining showed that under normal conditions, BTLA deficiency did not promote the proliferation of hepatocytes, but the proliferation of cells from $BTLA^{-/-}$ mice after IRI was reduced. This may be because there is too little damage in $BTLA^{-/-}$ mice after hepatic IRI, and most of the liver tissue did not show IRI-induced reactive proliferation of hepatocytes (Figure 4F, I). Taken together, these findings revealed that BTLA deficiency remarkably relieves hepatic injury after IRI.

Subsequently, we examined the changes in aHSC in mice. Compared with $BTLA^{+/+}$ mice, the expression of α-SMA and COL1A1 increased dramatically after hepatic IRI in $BTLA^{-/-}$ mice (Figure 4K, Supplemental Figures 4g, 4h, http://links.lww.com/HC9/A913). IHC staining revealed that α-SMA-positive HSCs increased significantly in $BTLA^{-/-}$ mice, mainly in the necrotic area (Figure 4F, J). Surprisingly, only a few apoptotic cells were seen in this section, but many proliferating cells surrounded the aHSC. Collectively, BTLA deficiency contributes to the local accumulation of aHSC during hepatic IRI, which protects hepatocytes from apoptosis and inflammation and promotes liver regeneration.

Depletion of aHSC reverses the protective effect of BTLA deficiency in mice

To further demonstrate the beneficial roles of BTLA deficiency based on the activation of HSCs, we

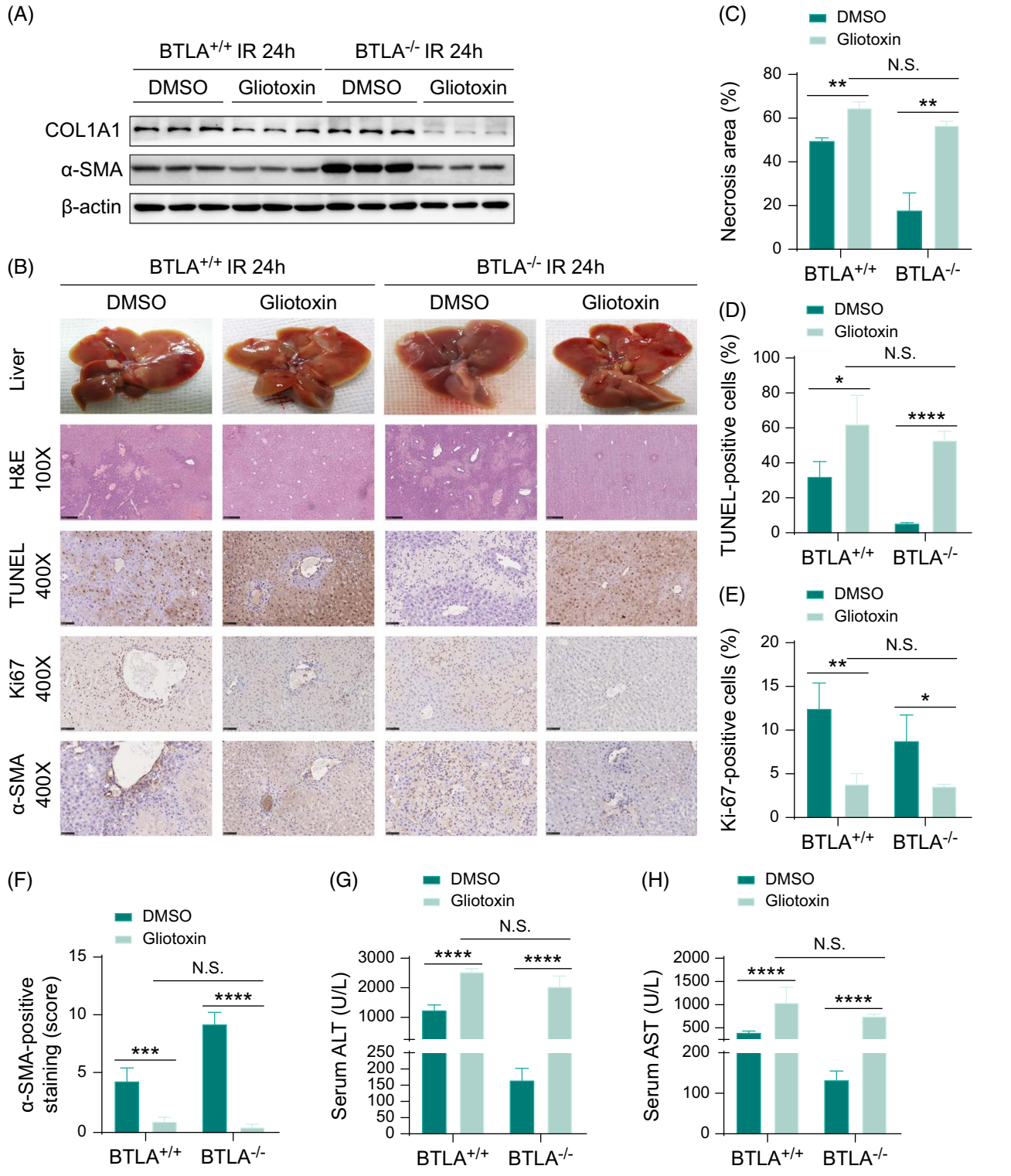

FIGURE 5 Depletion of aHSC reversed the protective effect of BTLA deficiency in mice. (A) Western blot analysis of COL1A1 and α-SMA expression in liver tissues from wild-type mice or BTLA$^{-/-}$ mice subjected to ischemia for 90 minutes, followed by reperfusion for 24 hours, in which mice were treated with DMSO or 3 mg/kg gliotoxin (n = 3/group). (B) The gross morphology (necrotic change), H&E staining (magnification ×100), TUNEL staining (brown color indicative of necrosis/apoptosis; magnification ×400), Ki-67 staining (brown color indicative of proliferation; magnification ×400), and α-SMA staining (brown color indicating aHSC deposition; magnification ×400) results for liver tissues from wild-type mice or BTLA−/− mice; (C), (D), (E), and (F) The corresponding quantitative analysis results are shown. Serum (G) ALT and (H) AST in livers (n = 3–4/group). All data are presented as the mean ± SD, * $p < 0.05$, ** $p < 0.01$, *** $p < 0.001$, **** $p < 0.0001$. Abbreviations: aHSC, activated HSCs; ALT, alanine aminotransferase; AST, aspartate aminotransferase; BTLA, B and T lymphocyte attenuators; BTLA−/−, BLTA-deficient; COL1A1, collagen type I alpha 1; H&E, hematoxylin and eosin; IR, ischemia-reperfusion; N.S., nonsignificant; α-SMA (ACTA2), α-smooth muscle actin.

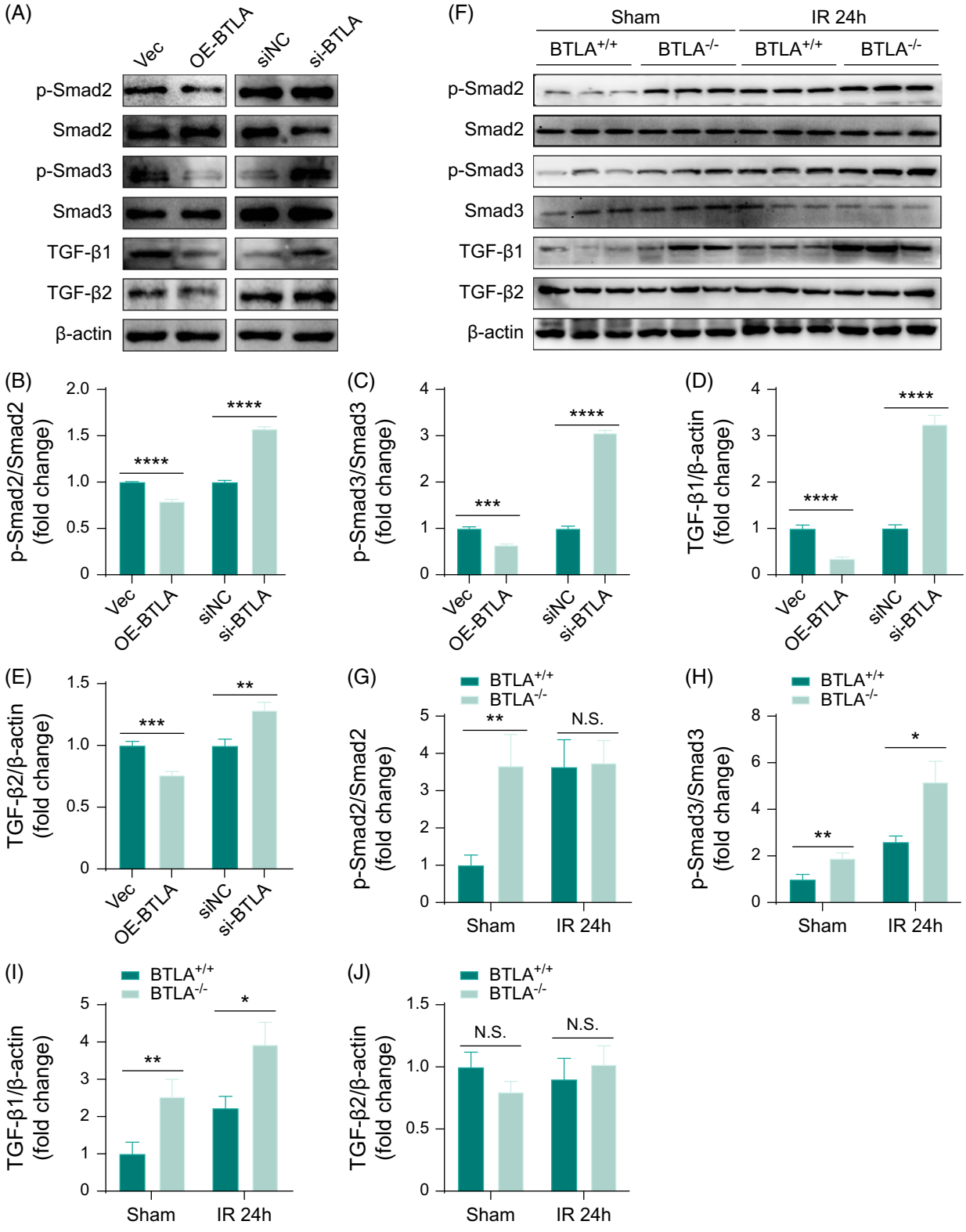

FIGURE 6 BTLA-regulated HSC activation through the TGF-βsignaling pathway. (a) Western blot showing expression of TGFβ1, TGFβ2, phosphorylation Smad2/total Smad2, and phosphorylation Smad3/total Smad3 in LX-2 cells subjected to transfected with empty-vector control or siNC, and transfected with BTLA overexpression or siRNAs; (B), (C), (D), and (E) The corresponding quantitative analysis results. (F) Western blot showing expression of TGFβ1, TGFβ2, phosphorylation Smad2/total Smad2, and phosphorylation Smad3/total Smad3 in liver tissues from wild-type mice or BTLA−/− mice subjected to sham treatment or IRI (n = 3/group); (G), (H), (I), and (J) The corresponding quantitative analysis results. All data are presented as the mean ± SD, * $p < 0.05$, ** $p < 0.01$, *** $p < 0.001$, **** $p < 0.0001$. Abbreviations: BTLA, B and T lymphocyte attenuators; BTLA−/−, BLTA-deficient; IRI, ischemia-reperfusion injury; N.S., nonsignificant.

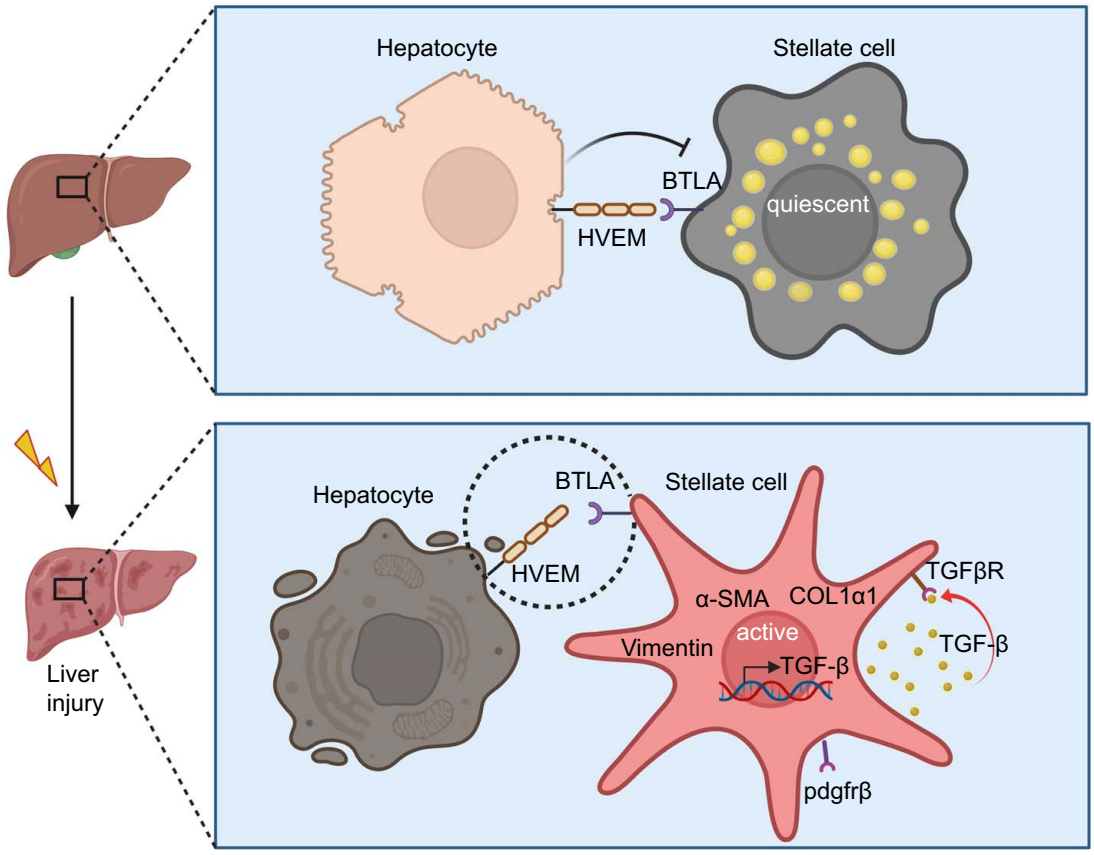

FIGURE 7 The potential mechanism by which BTLA regulates the activation of HSCs. We speculate that HVEM expressed on hepatocytes can bind with BTLA expressed on HSCs to trigger inhibitory signals and maintain the quiescent state of HSCs in the liver. Hepatocyte injury or apoptosis caused by IRI will result in HSC activation. Abbreviations: BTLA, B and T lymphocyte attenuator; HVEM, herpes virus entry mediator; α-SMA (ACTA2), α-smooth muscle actin; COL1A1, collagen type I alpha 1; Pdgfrβ, platelet-derived growth factor receptor beta; TGFβR, transforming growth factor beta receptor; TGF-β, transforming growth factor beta.

designed a rescue experiment in which aHSC in BTLA$^{-/-}$ mice were depleted. Western blot analysis showed satisfactory depletion of aHSC in mice treated with gliotoxin. The expression of α-SMA and COL1A1 were significantly lower in the gliotoxin-treated than in DMSO-treated controls (Figure 5A, Supplemental Figures 5a, 5b, http://links.lww.com/HC9/A914). Compared with BTLA$^{+/+}$mice, the liver damage in the BTLA$^{-/-}$ mice was more severe after depletion of the aHSC because serum ALT/AST levels were higher in this group of mice (Figure 5G, H). The expression of pro-inflammatory cytokines (IL-6, IL-18, IL-23, IL-12p40, and IL-12p70) and chemokines (CXCL1 and CCL17) was higher in the gliotoxin-treated group (Supplemental Figure 5c, http://links.lww.com/HC9/A914). Larger areas of necrosis and higher hepatocyte apoptosis, but lower expression of anti-inflammatory cytokines (TGF-β1) (Figure 5B-D, Supplemental Figure 5c, http://links.lww.com/HC9/A914), were also observed in the gliotoxin-treated group. These results suggested that the protective role of BTLA deficiency on hepatic IRI was largely reversed after the depletion of aHSC.

BTLA regulates HSC activation through the TGF-β1/Smad2/3 signal pathway

TGF-β signaling pathway plays a central role in regulating the activation of HSCs.[31] Therefore, we hypothesized that BTLA might regulate the activation of HSCs through the TGF-β signaling pathway. We first measured the levels of TGF-β/Smad2/3 in vitro. It was observed that the levels of TGF-β1/2, phosphorylation (p)-Smad2, and p-Smad3 were significantly decreased in LX-2 cells overexpressing BTLA, whereas they were significantly elevated in LX-2 cells knocking down BTLA (Figure 6A-E). These in vitro results suggest that BTLA regulates HSC activation through the TGF-β/Smad2/3 signaling pathway.

The role of BTLA in regulating TGF-β expression was confirmed with in vivo IRI mice models. Regardless of hepatic IRI status, compared with BTLA$^{+/+}$, the level of TGF-β1 protein was significantly higher in BTLA$^{-/-}$ mice. The ratio of p-Smad2/total Smad2 and p-Smad3/total Smad3 was high in BTLA$^{-/-}$ mice, but no difference was observed on the level of TGF-β2, suggesting that BTLA deficiency activated TGF-β1/Smad2/3 pathway in

mice (Figure 6F-J). Overall, BTLA inhibited the activation of HSCs by inhibiting the TGF-β1/Smad2/3 pathway.

DISCUSSION

Increasing evidence has demonstrated the involvement of HSCs in IRI recovery and regeneration after IRI.[9–13] However, their function on the liver after IRI had remained controversial. Liu et al[10] reported the destructive effect of activated HSCs on the liver as evidenced by the finding that YAP inhibition significantly delayed hepatic repair and potentiated HSC activation, which enhanced chronic injury and liver fibrosis at 7 days post-IRI. However, its effect on acute injury of IRI was not revealed. Jameel et al[11] showed that the secretion of antioxidant proteins mediates the protective effect of HSCs on hepatocytes. In the present study, we focused on the early stage (within 24 h) of IRI to provide ways of preventing sustained and acute side effects of hepatic IRI. Herein, our mice model revealed that activation of HSCs occurred 6 hours post-ischemia after reperfusion for 90 minutes and gradually increased at 24 hours post-reperfusion. The pentobarbital dose used was based on previous literature.[32] Moreover, we found that the site with more αHSC accumulation was less damaged. The "loss-of-function" experiments of depleting aHSC through gliotoxin treatment further confirmed the protective role of HSC activation at the early phase of hepatic IRI. These results showed that aHSC protected the liver from acute injury after hepatic IRI.

RNA-seq analysis was performed to identify differentially expressed genes that potentially regulate the activation of HSCs between primary mouse aHSC and qHSCs. It was found that BTLA, which participates in regulating the proliferation and activation of various immune cells,[14,15] is also expressed in HSCs and was remarkably low in aHSC. RT-qPCR and western blot analyses revealed comparable findings. Accordingly, BTLA could be a potential biomarker for distinguishing qHSCs from aHSC. In light of the low expression of BTLA in aHSC, we hypothesized that BTLA participates in the activation of HSCs. Overexpression and silencing of BTLA in LX-2 cells revealed that BTLA negatively regulated the activation and apoptosis of HSCs. In addition, BTLA was significantly decreased in both primary mHSCs and the LX-2 cells when processed in vitro with HR stimulation (mimicking the action of IRI), respectively. Further, in vivo experiments using the hepatic IRI model confirmed this phenomenon. Thus, it is reasonable that BTLA may act as a molecular switch to regulate the activation of HSCs, and once the BTLA switch fails, HSC activation increases.

BTLA, a co-inhibitory molecule similar to PD1 and cytotoxic T lymphocyte ag-4, is extensively expressed on the surface of many immune cells, including T cells, B cells, natural killer T cells, natural killer cells, dendritic cells, macrophages, and monocytes.[14,15] However, the relationship between BTLA and HSCs has not been elucidated. Additionally, studies have shown that BTLA is related to acquired immune response[33–35] and immune response to infectious pathogens,[35,36] but its role in IRI remains unclear. PD1 and CTLA4, members of the CD28 family, alleviate IRI-induced liver injury by reducing inflammation.[20–22] Based on these studies and our findings above, we speculated that BTLA might also participate in the hepatic IRI process and activation of HSCs (Figure 7). Significant alleviation of liver injury was observed, including decreased serum ALT/AST level, alleviated inflammation, decreased necrosis, suppressed apoptosis, and upregulated proliferation in $BTLA^{-/-}$ mice after hepatic IRI. Furthermore, the expression of α-SMA and COL1A1 was relatively higher in $BTLA^{-/-}$ mice under both normal conditions and hepatic IRI stress. Surprisingly, the depletion of aHSC with gliotoxin reversed the protective role of BTLA deficiency on hepatic IRI. Therefore, we concluded that BTLA deficiency protects the liver against IRI by promoting HSC activation.

However, how does aHSC protect the liver from IRI? This was worthy of further study. Excessive inflammation induces apoptosis of hepatocytes and liver necrosis, directly causing liver injury and affecting the regeneration and recovery of liver damage,[29,37] consistent with our findings. HSCs can directly secrete inflammatory cytokines and indirectly affect the accumulation of inflammatory cytokines by interacting with immune cells.[38] Therefore, we focused on the fluctuation of inflammatory cytokines and chemokines using mice models. We found that most serum pro-inflammatory cytokines and chemokines were prominently high, and anti-inflammatory cytokines, especially TGF-β1, were remarkably low after aHSC depletion. An opposite effect was observed in $BTLA^{-/-}$ mice. TGF-β1 signaling pathway is involved in IRI of different organs.[39] Our previous study[40] showed that activation of the TGF-β1 signaling pathway protects the liver from hepatic IRI, evidenced by aggravated hepatic injury in Smad3 knockout mice. Herein, both our in vivo and in vitro experiments have confirmed the involvement of the TGF-β1/Smad3 signaling pathway in BTLA-mediated HSC activation.

This study had some limitations. Firstly, we only analyzed the role of aHSC in the IRI process. The role of other cells, such as B cells, T cells, and macrophages, among others, in IRI, was not explored in this study. The research direction could be explored in our future works. Moreover, how BTLA is downregulated after traumatic stimulation is still unknown. Additionally, our study only found that BTLA can regulate the activation of HSCs through the TGF-β1 signaling pathway, but the specific mechanism still needs to be

clarified. Finally, our in vitro results showed that the overexpression of BTLA promotes the apoptosis and inactivation of HSCs. Whether increasing the expression of BTLA can treat chronic liver fibrosis is a clinical problem worth exploring.

In conclusion, BTLA deficiency promotes the activation of HSCs by regulating TGF-β1 signaling, alleviating hepatic IRI. Our results offered novel insights into liver IRI and revealed that targeting BTLA may serve as a latent method to prevent IRI.

AUTHOR CONTRIBUTIONS

Xiaoyun Shen: Conception and design, funding, analysis, revising the manuscript, and final approval of the version to be published. Rongyun Mai: Carry out experiments and writing original draft. Xiao Han: Validation. Yifan Wang and Qi Wang: Resources. Tong Ji: Project guidance. Yifan Tong: Methodology. Ping Chen: Data Curation. Jia Zhao: Investigation. Xiaoyan He: Formal analysis. Tong Wen: Software. Rong Liang: Visualization. Yan Lin: Methodology. Xiujun Cai and Xiaoling Luo: Investigation, Project administration, Resources, and Supervision of the study. All authors performed data analysis and interpretation and read and approved the final manuscript.

The authors Xiaoyun Shen and Rongyun Mai contributed equally to this work.

ACKNOWLEDGMENTS

The authors thank Dr Xinping Huang and Master Haixia Li for their participation in guiding the isolation of primary mouse stellate cells.

FUNDING INFORMATION

This work was supported by the National Natural Science Foundation of China [grant number 81702854].

AVAILABILITY OF DATA AND MATERIALS

The datasets used and/or analyzed during the present study are available from the corresponding author upon reasonable request.

ETHICS APPROVAL AND CONSENT TO PARTICIPATE

All animal experiments included in this protocol adhere to the Animal Research: Reporting In Vivo Experiments guidelines and have been approved by the Animal Testing Ethics Committee of Zhejiang University approval (Project Approval Number: ZJU20170115).

CONFLICTS OF INTEREST

The authors have no conflicts to report.

ORCID

Xiaoyun Shen https://orcid.org/0000–0003–2098–9728
Rongyun Mai https://orcid.org/0009–0008–9830–0197
Tong Wen https://orcid.org/0000–0003–0937–0086
Rong Liang https://orcid.org/0000–0003–0343–3277
Yan Lin https://orcid.org/0000–0001–8034–5946

REFERENCES

1. Izuishi K, Tsung A, Hossain MA, Fujiwara M, Wakabayashi H, Masaki T, et al. Ischemic preconditioning of the murine liver protects through the Akt kinase pathway. Hepatology. 2006;44:573–80.
2. Li Z, Cai J, Zheng J, Liang X. Repeated laparoscopic liver resection using ICG fluorescent imaging for recurrent liver cancer. Laparosc Endosc Robot Surg. 2022;5:19–24.
3. Peralta C, Jimenez-Castro MB, Gracia-Sancho J. Hepatic ischemia and reperfusion injury: effects on the liver sinusoidal milieu. J Hepatol. 2013;59:1094–106.
4. Kawka M, Gall TM, Jiao LR. Minimum invasive associating liver partition and portal vein ligation for staged hepatectomy. Laparosc Endosc Robot Surg. 2020;3:5.
5. Friedman SL. Hepatic stellate cells: Protean, multifunctional, and enigmatic cells of the liver. Physiol Rev. 2008;88:125–72.
6. Tsuchida T, Friedman SL. Mechanisms of hepatic stellate cell activation. Nat Rev Gastroenterol Hepatol. 2017;14:397–411.
7. Mederacke I, Hsu CC, Troeger JS, Huebener P, Mu X, Dapito DH, et al. Fate tracing reveals hepatic stellate cells as dominant contributors to liver fibrosis independent of its aetiology. Nat Commun. 2013;4:2823.
8. Gabbiani G. The myofibroblast in wound healing and fibrocontractive diseases. J Pathol. 2003;200:500–3.
9. Stewart RK, Dangi A, Huang C, Murase N, Kimura S, Stolz DB, et al. A novel mouse model of depletion of stellate cells clarifies their role in ischemia/reperfusion- and endotoxin-induced acute liver injury. J Hepatol. 2014;60:298–305.
10. Liu Y, Lu T, Zhang C, Xu J, Xue Z, Busuttil RW, et al. Activation of YAP attenuates hepatic damage and fibrosis in liver ischemia-reperfusion injury. J Hepatol. 2019;71:719–30.
11. Jameel NM, Thirunavukkarasu C, Murase N, Cascio M, Prelich J, Yang S, et al. Constitutive release of powerful antioxidant-scavenging activity by hepatic stellate cells: Protection of hepatocytes from ischemia/reperfusion injury. Liver Transpl. 2010;16:1400–9.
12. Konishi T, Schuster RM, Lentsch AB. Liver repair and regeneration after ischemia-reperfusion injury is associated with prolonged fibrosis. Am J Physiol Gastrointest Liver Physiol. 2019;316:G323–31.
13. Konishi T, Schuster RM, Lentsch AB. Proliferation of hepatic stellate cells, mediated by YAP and TAZ, contributes to liver repair and regeneration after liver ischemia-reperfusion injury. Am J Physiol Gastrointest Liver Physiol. 2018;314:G471–82.
14. Watanabe N, Gavrieli M, Sedy JR, Yang J, Fallarino F, Loftin SK, et al. BTLA is a lymphocyte inhibitory receptor with similarities to CTLA-4 and PD-1. Nat Immunol. 2003;4:670–9.
15. Murphy TL, Murphy KM. Slow down and survive: Enigmatic immunoregulation by BTLA and HVEM. Annu Rev Immunol. 2010;28:389–411.
16. Demerle C, Gorvel L, Olive D. BTLA-HVEM couple in health and diseases: Insights for immunotherapy in lung cancer. Front Oncol. 2021;11:682007.
17. Cai G, Freeman GJ. The CD160, BTLA, LIGHT/HVEM pathway: A bidirectional switch regulating T-cell activation. Immunol Rev. 2009;229:244–58.
18. Murphy KM, Nelson CA, Sedy JR. Balancing co-stimulation and inhibition with BTLA and HVEM. Nat Rev Immunol. 2006;6:671–81.

19. Ning Z, Liu K, Xiong H. Roles of BTLA in Immunity and Immune Disorders. Front Immunol. 2021;12:654960.
20. Ji H, Shen X, Gao F, Ke B, Freitas MCS, Uchida Y, et al. Programmed death-1/B7-H1 negative costimulation protects mouse liver against ischemia and reperfusion injury. Hepatology. 2010;52:1380–9.
21. Takada M, Chandraker A, Nadeau KC, Sayegh MH, Tilney NL. The role of the B7 costimulatory pathway in experimental cold ischemia/reperfusion injury. J Clin Invest. 1997;100: 1199–203.
22. Chandraker A, Takada M, Nadeau KC, Peach R, Tilney NL, Sayegh MH. CD28-b7 blockade in organ dysfunction secondary to cold ischemia/reperfusion injury. Kidney Int. 1997;52:1678–84.
23. Guo WZ, Fang HB, Cao SL, Chen SY, Li J, Shi JH, et al. Six-transmembrane epithelial antigen of the prostate 3 deficiency in hepatocytes protects the liver against ischemia-reperfusion injury by suppressing transforming growth factor-beta-activated kinase 1. Hepatology. 2020;71:1037–54.
24. Nejak-Bowen KN, Orr AV, Bowen WC Jr, Michalopoulos GK. Gliotoxin-induced changes in rat liver regeneration after partial hepatectomy. Liver Int. 2013;33:1044–55.
25. Elsharkawy AM, Oakley F, Mann DA. The role and regulation of hepatic stellate cell apoptosis in reversal of liver fibrosis. Apoptosis. 2005;10:927–39.
26. Wang SS, Tang XT, Lin M, Yuan J, Peng YJ, Yin X, et al. Perivenous stellate cells are the main source of myofibroblasts and cancer-associated fibroblasts formed after chronic liver injuries. Hepatology. 2021;74:1578–94.
27. Yan ZZ, Huang YP, Wang X, Wang HP, Ren F, Tian RF, et al. Integrated omics reveals tollip as an regulator and therapeutic target for hepatic ischemia-reperfusion injury in mice. Hepatology. 2019;70:1750–69.
28. Livak KJ, Schmittgen TD. Analysis of relative gene expression data using real-time quantitative PCR and the 2(-Delta Delta C (T)) Method. Methods. 2001;25:402–8.
29. Zhang JK, Ding MJ, Liu H, Shi JH, Wang ZH, Wen PH, et al. Regulator of G-protein signaling 14 protects the liver from ischemia-reperfusion injury by suppressing TGF-beta-activated kinase 1 activation. Hepatology. 2022;75:338–52.
30. Sedy JR, Gavrieli M, Potter KG, Hurchla MA, Lindsley RC, Hildner K, et al. B and T lymphocyte attenuator regulates T cell activation through interaction with herpesvirus entry mediator. Nat Immunol. 2005;6:90–8.
31. Hellerbrand C, Stefanovic B, Giordano F, Burchardt ER, Brenner DA. The role of TGFbeta1 in initiating hepatic stellate cell activation in vivo. J Hepatol. 1999;30:77–87.
32. Sun L, Wu Q, Nie Y, Cheng N, Wang R, Wang G, et al. A role for MK2 in enhancing neutrophil-derived ROS production and aggravating liver ischemia/reperfusion injury. Front Immunol. 2018;9:2610.
33. Steinberg MW, Turovskaya O, Shaikh RB, Kim G, McCole DF, Pfeffer K, et al. A crucial role for HVEM and BTLA in preventing intestinal inflammation. J Exp Med. 2008;205:1463–76.
34. Iwata A, Watanabe N, Oya Y, Owada T, Ikeda K, Suto A, et al. Protective roles of B and T lymphocyte attenuator in NKT cell-mediated experimental hepatitis. J Immunol. 2010;184:127–33.
35. Sun Y, Brown NK, Ruddy MJ, Miller ML, Lee Y, Wang Y, et al. B and T lymphocyte attenuator tempers early infection immunity. J Immunol. 2009;183:1946–51.
36. Adler G, Steeg C, Pfeffer K, Murphy TL, Murphy KM, Langhorne J, et al. B and T lymphocyte attenuator restricts the protective immune response against experimental malaria. J Immunol. 2011;187:5310–9.
37. Lu L, Zhou H, Ni M, Wang X, Busuttil R, Kupiec-Weglinski J, et al. Innate immune regulations and liver ischemia-reperfusion injury. Transplantation. 2016;100:2601–10.
38. Koyama Y, Brenner DA. Liver inflammation and fibrosis. J Clin Invest. 2017;127:55–64.
39. Derynck R, Zhang YE. Smad-dependent and smad-independent pathways in TGF-beta family signalling. Nature. 2003;425: 577–84.
40. Li H, Shen X, Tong Y, Ji T, Feng Y, Tang Y, et al. Aggravation of hepatic ischemiareperfusion injury with increased inflammatory cell infiltration is associated with the TGFbeta/Smad3 signaling pathway. Mol Med Rep. 2021;24:580.

How to cite this article: Shen X, Mai R, Han X, Wang Q, Wang Y, Ji T, et al. BTLA deficiency promotes HSC activation and protects against hepatic ischemia-reperfusion injury. Hepatol Commun. 2024;8:e0449. https://doi.org/10.1097/HC9.0000000000000449